Mon. Not. R. Astron. Soc. **275,** 703–710 (1995)

Polarimetry of the ultraviolet continua of southern radio galaxies

M. Shaw,[1] C. Tadhunter,[1] R. Dickson[1] and R. Morganti[2,3]

[1]*Department of Physics, University of Sheffield, The Hicks Building, Hounsfield Road, Sheffield S3 7RH*
[2]*Instituto di Radioastronomia, CNR, via Gobetti 101, Bologna, Italy*
[3]*Australia Telescope National Facility, CSIRO, Epping, NSW 2121, Australia*

Accepted 1995 February 10. Received 1994 December 20; in original form 1994 July 21

ABSTRACT

This paper reports new *B*-band polarimetry measurements for four intermediate-redshift ($0.3 < z < 0.7$) southern radio galaxies. Deep optical spectra show that three of these objects are broad-line radio galaxies, while the fourth is a narrow-line radio galaxy.

Despite the fact that the measurements were made in the rest-frame ultraviolet (UV) in each object, and that emission-line contamination is small, we find that the majority of objects display low intrinsic continuum polarization. In two of the broad-line objects (PKS 1602+01 and PKS 2135−20), this may result from our viewing the broad-line region directly. The significant polarization measure, and corresponding polarization orientation, in the narrow-line object PKS 2250−41 is most consistent with scattering of light from the active nucleus.

We therefore identify a diversity of UV polarization properties in powerful radio galaxies at intermediate redshifts. Not all radio galaxies possess large intrinsic polarizations. Therefore the UV excesses observed in these objects are unlikely to result solely from scattered light.

Key words: polarization – techniques: polarimetric – galaxies: active – ultraviolet: galaxies.

1 INTRODUCTION

An understanding of the nature of the ultraviolet (UV) continuum in powerful radio galaxies lies at the heart of many investigations of these enigmatic objects.

An important early result was the demonstration that the high-redshift ($z > 0.5$) radio galaxies are bluer than early-type galaxies at low redshifts (Lilly & Longair 1984). This led to speculation that the UV excess was a sign of recent star formation and evolutionary processes in the host galaxies. The subsequent discovery of a close alignment between radio and optical/UV structures suggests, however, that, if recent star formation has indeed taken place, then it must be related in some way to the extended radio structures (Chambers, Miley & van Breugel 1987; McCarthy et al. 1987). As a result, there have been attempts to model the UV structures in terms of a jet-induced mechanism in which the radio jet promotes star formation by compressing the ambient medium in the host galaxies (Begelman & Cioffe 1989; de Young 1989; Rees 1989).

The recent development of anisotropy-based unified schemes for radio galaxies (Barthel 1989), and the recognition that powerful radio galaxies are likely to have powerful active galactic nuclei (AGN), has led to some retrenchment from the idea that the UV excess is solely due to starlight. In particular, it has been proposed that the aligned continuum structures represent light scattered out of the radiation cones of hidden AGN by electrons or dust in the interstellar medium (ISM) or intergalactic medium (IGM) (Tadhunter, Fosbury & di Serego Alighieri 1988; Fabian 1989). This is supported by observations which show strong evidence for scattered light in the form of large UV polarization with *E*-vectors aligned close to perpendicular to the UV structure axes (Tadhunter et al. 1992; Cimatti et al. 1993, and references therein).

It is clear, therefore, that scattered light makes a significant contribution to the UV excess in several powerful radio galaxies. The main question that remains is: does the scattered light *dominate* the UV continuum in *most* high-redshift radio galaxies, or is there a role for other continuum emission mechanisms? Several alternative mechanisms exist, including emission from young stars produced either as a result of evolutionary processes or jet-induced star formation (e.g. Rees 1989), nebular continuum emission associated

with the warm emission-line clouds (Dickson et al. 1995), inverse Compton scattering (e.g. Daley 1992), and direct or transmitted AGN light.

When determining the exact proportion of scattered light we are faced with several problems. First, the observed fractional polarization only provides a *lower limit* to the proportion of scattered light at a particular wavelength, the measured value depending on the geometry, as well as the nature and optical depth of the scattering medium. Secondly, there will be some dilution of the polarization by the (unpolarized) light of the old stellar populations in the host galaxies. This dilution will affect all wavelengths but will be particularly severe for optical–infrared rest wavelengths (Tadhunter et al. 1992; Cimatti et al. 1993). Finally, because the polarization measurements are difficult, there has been a natural tendency to concentrate on the brightest, most spectacular objects. Polarization measurements of a complete, optically unbiased sample of powerful radio galaxies do not yet exist.

In this paper, we present new polarization observations of four southern radio galaxies. Our observations serve to emphasize that a diversity of UV continuum emission mechanisms exists in powerful radio galaxies.

2 OBSERVATIONS

2.1 Sample selection

The four objects discussed in this paper are listed in Table 1. They constitute a subset of the complete 2-Jy southern radio galaxy sample of Tadhunter et al. (1993). All have redshifts in excess of 0.3, contain steep spectrum radio sources (Wall & Peacock 1985), and, based on the rest-frame $(U-B)$ colours derived from spectroscopy, show UV excesses compared with early-type galaxies at low redshifts (see Section 3.2). PKS 2135 − 20 is a compact steep spectrum (CSS) radio source, but the other three objects are associated with classic double-lobed radio sources (see Duncan & Sproats 1992; Morganti, Killeen & Tadhunter 1993). Based on the previous spectroscopic observations reported in Tadhunter et al. (1993), all the objects were known to have strong narrow emission-line spectra prior to the observations.

As is the case with most other data sets observed polarimetrically, our sample is heterogeneous and there were a variety of motivations for the sample selection. PKS 2135 − 20 and PKS 1547 − 79 were observed because they are brighter in the continuum than other radio galaxies at similar redshift; PKS 1602 + 01 was observed because it shows a hint of a broad wing to Hβ which may be a sign of a scattered quasar; and PKS 2250 − 41 was observed because it shows particularly interesting extended structures (Tadhunter et al. 1994).

2.2 Data acquisition and reduction

The observational data were acquired between 1993 July 20 and 24 using the EFOSC in direct imaging, spectroscopic and imaging polarimetric modes on the ESO 3.6-m telescope. Use of the Tek 26 CCD as detector yields a pixel scale of 0.61 arcsec for a field-of-view of 5.1 arcmin^2.

The 25 individual bias frames acquired throughout the run were found to be equivalent to high accuracy (the standard deviation being ~0.7 per cent of the mean value). They were thus median filtered. Bias subtraction was undertaken using the resulting average bias frame, scaled to match the mean counts in the overscan regions of each object frame. As no appreciable dark current was noted in these data [a mean of 0.01 (±8.09) counts in 30 minutes of integration], no dark current correction was applied.

The data were flat-fielded using high signal-to-noise ratio sky flats median-filtered from individual frames taken throughout the run. Such flat-fields were not only acquired using the appropriate filters, but were taken through the same polarization optics used for the object/star frames. The 20-arcsec Wollaston prism was used throughout, as was the *B* filter for the object frames. An aperture mask was used in the majority of observations to minimize the likelihood of contamination by superposition of nearby objects. To recover complete polarization information, object frames were acquired using four instrument position angles, each rotated 45° with respect to the previous observation. Integration times were 15 min in each of the four instrument position angles for each object. One such cycle was acquired for PKS 1547 − 79 and PKS 2135 − 20, and three cycles for PKS 1602 + 01 and PKS 2250 − 41.

Table 1. Properties of the present subsample.

object	z	Optical classification	night observed	rest frame range (Angstrom)	(U-B) (mag.)	m_B (mag.)	aperture (arcsec)	comments
PKS1547–79	0.483	BLRG	2	2613 – 3300	−0.50(±0.02)	20.21(±0.01)	6.1	
PKS1602+01	0.462	BLRG	2(×2), 4	2650 – 3347	−0.27(±0.06)	21.54(±0.04)	6.1	
PKS2135–20	0.635	BLRG	4	2370 – 2993	−0.29(±0.04)	20.97(±0.01)	4.9	
PKS2250–41	0.310	NLRG	1, 2, 4	2958 – 3736	+0.09(±0.05)	21.20(±0.02)	4.9	nucleus
					−0.86(±0.05)	21.19(±0.02)	4.9	W. lobe

Notes to Table 1.
Column 2: redshifts from Tadhunter et al. (1993).
Column 3: optical classifications derived by inspection of the spectra presented in this paper.
Column 4: nights 1, 2 and 4 are 1993 July 20–21, 21–22 and 23–24 respectively.
Column 5: FWHM of the *B*-band filter, shifted to the rest wavelengths of each object using the redshifts in column 2.
Column 6: $(U-B)$ continuum colour indices derived from our spectra as outlined in Section 3.2. The quoted uncertainties are random errors derived from the mean continuum fluxes in each object. They do not reflect the likely systematic error in flux calibration which we estimate to be $< \pm 0.1$ mag.
Columns 7 and 8: apparent (B) magnitudes, and associated errors, derived from our calibration polarization images within the specified aperture diameters.

Observations of five photometric standard stars during the same run indicate that photometric conditions prevailed at all times – the derived standard deviations on the mean *B*-band magnitude zero-point being ±0.06 mag (derived from 15 independent estimates over all four nights). The atmospheric seeing, as determined from field stars on direct EFOSC images, varied from 1.2 to 1.9 arcsec (FWHM) throughout the run. Observations of the standard star LTT 7379 were also acquired through the polarization optics over several nights to provide a photometric calibration of our polarization images.

Polarization calibration was facilitated by observations of the polarized standard star HD 126593 [$P=5.02$ (±0.01) per cent, Turnshek et al. 1990], while instrument polarization was corrected for by observing the unpolarized star HD 176425 [$P=0.02$ (±0.01) per cent, Turnshek et al. 1990]. As both of these stars are bright, they were observed through a narrow-band (62 Å) Hα filter. Only two instrument position angles were acquired for the standard stars. In consequence, polarization measurements for HD 126593 were derived using the technique outlined by di Serego Alighieri (1989). The percentage polarization thus derived was 4.9 (±0.4) per cent respectively, in excellent agreement with the published measures (Turnshek et al. 1990).

Spectra of PKS 1547−79, PKS 2135−20 and PKS 2250−41 were acquired on the same run as the images discussed above using EFOSC in spectroscopic mode. They comprise short (15 min) and long (20–60 min) spectra using R300 and B300 grisms respectively, and were obtained using a 2-arcsec slit resulting in a spectral resolution of 20 Å FWHM. These spectra were reduced using standard methods, and calibrated using numerous observations of the spectrophotometric standard stars LTT 377, LTT 7379, LTT 9239, LTT 9491 and BPM 16274. We estimate that systematic errors, resulting from uncertainties in the flux calibrating procedure, are at most ±10 per cent.

Spectra were also acquired for 3C 411, PKS 2135−20 and PKS 1602+01 on 1992 July 29 and 30 using the red arm of ISIS with the EEV3 CCD on the WHT 4.2-m telescope at La Palma. Use of a 1.5–2.0 arcsec slit resulted in wavelength resolution of 12–16 Å, with a flux calibration uncertainty similar to that for the EFOSC data. The relevance of our spectroscopy of 3C 411 will be addressed in Section 4 below.

3 POLARIZATION MEASUREMENTS FOR THE RADIO GALAXIES

3.1 Techniques

Polarization measures for each of the objects listed in Table 1 were derived using the technique outlined in Tinbergen & Rutten (1992), involving the ratios of 'o'- and 'e'-ray fluxes at each of four telescope rotator position angles offset by 45°. This approach is preferable to that of di Serego Alighieri (1989) as it automatically corrects for intrinsic instrumental polarization.

An accurate estimate of the sky is vital in polarization measurements. The sky background within each 'o'- and 'e'-ray image was determined using ~5-arcsec-diameter apertures throughout. This aperture size was found to be the optimum necessary to minimize statistical fluctuations which would unduly influence measures in smaller apertures, while also ensuring the sky values remain uncontaminated by flux from the target objects or by other galaxies or stars. Where necessary, the sky measures derived were rescaled to those apertures adopted on the target objects themselves. Typically eight sky apertures – in positions surrounding each object – were used to derive a mean sky background measure. Estimates of the associated uncertainties were provided by the corresponding standard deviations on the means. For the integrated (object + sky) fluxes within each source, errors were assigned on the basis of Poisson statistics in the usual manner. The errors quoted throughout this paper result from formal propagation of uncertainties derived from the combined sky and Poisson errors in each case.

An assumption implicit within our sky estimates, as well as their corresponding errors, is that of a flat underlying sky background. This is a valid approximtion in observations of PKS 1602+01, PKS 2135−20 and PKS 2250−41: the standard deviation on the average sky measures, expressed as a fraction of these mean values and averaged between both 'o'- and 'e'-rays for each night, is 0.12 (±0.05) per cent. Such an assumption is, however, invalid for PKS 1547−79, where a bright nearby star leads to a significant slope in the sky background at an instrument position angle of 225°. Correction for this effect was undertaken by fitting the underlying sky in each 'o'- and 'e'-ray separately, after removal of all stars/galaxies, using a 2D spline surface. Both 'o'- and 'e'-ray surfaces were normalized to a median of unity, and divided into the original images prior to evaluation of the sky background or object polarization. Inclusion of the PKS 1547−79 sky measures thus derived have a nominal effect on the aforementioned standard deviation on the sky, increasing it to 0.13 (±0.06) per cent of the mean value. Moreover, the (object − sky) fluxes summed in both 'o' and 'e' rays are found to be consistent between each of the instrument position angles to within the associated errors.

To minimize uncertainties in the smallest apertures resulting from the relatively large pixel size used, polarization measures were derived using apertures located on the flux centroids of each object, these centroids being measured to an accuracy of $\lesssim 0.1$ arcsec.

The reliability of the measures thus derived were confirmed in all cases by detailed inspection of the pattern of (object − sky) fluxes in the different instrument rotator position angles. This allows one to identify spuriously large polarization measures resulting from, for example, cosmic ray contamination. Measured polarizations were thus only considered reliable in those cases for which a symmetric pattern, typical of that of a linearly polarized source, was observed. True polarization position angles were calculated on the basis of the sign of the Stokes Q and U parameters, after calibration using observations of the standard star HD 126593.

In those objects for which several polarization cycles were acquired (PKS 1602+01 and PKS 2250−41), final percentage polarization and corresponding position angle estimates were derived from weighted mean Stokes parameters from each independent cycle. The errors on each measure were evaluated by the usual propagation of uncertainties on the weighted mean Stokes parameters.

3.2 Results

The results derived for each of the programme objects are given in Table 2. We also tabulate the corresponding polarization measures derived after correcting for the positive bias in P_{obs} using the procedure outlined in Simmons & Stewart (1985). In the first instance, an estimate of the likely foreground contamination by aligned grains within our own Galaxy is afforded by inspection of the H I maps of Burstein & Heiles (1982). By adopting the conventional $P_{Galaxy}(V\text{-band}) \lesssim 8.6\,E(B-V)$ per cent mag^{-1} relation from Serkowski, Matthewson & Ford (1975), we find that the likely Galactic contribution to P_{obs} is $\lesssim 1.0$ per cent in all objects. Moreover, emission-line contamination of our B-band polarization measures is minimal in PKS 1547−79, PKS 1602+01 and PKS 2135−20: our EFOSC spectra indicate contamination by [Ne V] (λλ3426, 3346 Å) and/or Mg II (λ2800 Å) of $\lesssim 1.5$ per cent. The contamination is larger in PKS 2250−41 (Tadhunter et al. 1994) – the actual measures being cited below. The polarization measures quoted henceforth (and in Table 2) are corrected throughout for the degree of contamination estimated from our spectra, assuming the emission lines to be unpolarized. We discuss each object in turn below.

Table 2. Summary of derived polarization results in the present data set.

object	aperture diameter (arcsec)	(kpc)	P_{obs} (%)	Θ_{true} (deg.)	pattern ?	P_{true} (%)
PKS1547–79	6.1	85.7	3.0 (±0.7)	66 (±7)	yes	2.9 (±0.7)
	4.9	68.8	3.8 (±0.6)	66 (±4)	yes	3.8 (±0.6)
	3.7	52.0	4.7 (±0.5)	66 (±3)	yes	4.8 (±0.5)
	2.4	33.7	6.2 (±0.5)	66 (±2)	yes	6.2 (±0.5)
PKS1602+01	6.1	82.0	1.4 (±1.6)	109 (±32)	no	<4.8
	4.9	65.9	2.7 (±1.5)	94 (±14)	no	<4.5
	3.7	49.7	2.1 (±1.6)	100 (±17)	no	<4.8
	2.4	32.3	1.8 (±1.2)	119 (±22)	no	<3.6
PKS2135–20	4.9	90.5	0.6 (±0.9)	173 (±38)	no	<2.7
	3.7	68.3	0.5 (±0.7)	170 (±40)	no	<2.1
	2.4	44.3	1.3 (±0.7)	180 (±16)	no	<2.1
PKS2250–41 (nucleus)	6.1	55.0	3.7 (±0.8)	159 (±5)	yes	4.4 (±0.8)
	4.9	44.2	4.0 (±0.7)	156 (±5)	yes	4.9 (±0.7)
	3.7	33.4	4.0 (±0.7)	154 (±4)	yes	4.9 (±0.7)
	2.4	21.6	3.7 (±0.7)	152 (±5)	yes	4.5 (±0.7)
PKS2250–41 (W lobe)	6.1	55.0	1.5 (±0.9)	16 (±7)	no	<4.5
	4.9	44.2	1.5 (±0.7)	12 (±8)	no	<3.5
	3.7	33.4	1.7 (±0.7)	7 (±8)	no	<3.5
	2.4	21.6	1.7 (±0.8)	10 (±8)	no	<4.0

Notes to Table 2.
Column 3: linear aperture size on the source (kpc) derived using the redshifts in Table 1 and assuming an $H_0 = 50$ km s^{-1} Mpc^{-1} and a $q_0 = 0.0$.
Column 4: observed polarization measures derived as discussed in the text and uncorrected for any emission-line contamination.
Column 5: true polarization position angles (measured north through east) calibration using the polarization standard star observations as discussed in the text.
Column 6: identification of a pattern in (object − sky) fluxes consistent with that expected from a linearly polarized source (see Section 3.1 for details). In those cases where weighted means are cited (namely PKS 1602+01 and PKS 2250−41), the evidence for a valid pattern reflects the conclusions derived from the respective observations taken independently on each night.
Column 7: observed polarization measures in column 4 corrected for the positive bias in the Rice distribution using the formulation of Simmons & Stewart (1985). Values have also been corrected for emission-line contamination as outlined in the text. In cases where $P_{obs}/\sigma_{obs} \leq 1$, only 3σ upper limits to P_{true} are given.

3.2.1 *PKS 1547−79*

At 6 cm, this radio galaxy shows an archetypal double-lobed structure along a position angle (PA) of 24° (±5°) (Duncan & Sproats 1992; Burgess & Hunstead, private communication). A contour plot of a subregion from the calibrated B-band polarization image is presented in Fig. 1. Ellipse-fitting techniques applied to the 270° instrumental position angle frame after summing subimages from both 'o'- and 'e'-rays, yield a mean PA (over 2.1–5.2 arcsec diameter apertures) of 22°.0 (±7°.5) and a corresponding mean ellipticity of 0.9 (±0.02). Thus the optical and radio structure axes are close to parallel.

As Table 2 shows, this object is seemingly polarized in all apertures. Within the smallest (2.4-arcsec diameter) aperture, we measure a level of 6.2 (±0.5) per cent at an angle of 66° (±2°). Radio and polarization position angles therefore differ by 42° (±5°).

This galaxy is closer to the galactic plane than any other in the present sample. Unfortunately, estimates of foreground polarization in these data are difficult owing to there being relatively few unsaturated stars common to frames acquired at suitable instrument position angles. Measurements from the two most suitable stars yield polarizations of 1 (±0.4) per cent and 2.8 (±0.7) per cent within 3.7- and 7.4-arcsec-diameter apertures, respectively. The polarization position angles derived are within ±30° of that for PKS 1547−79. Therefore there exists the possibility of foreground contamination from within our own Galaxy. Although this does not concur with the implications of the H I measures in this region, it is also supported by similar measurements of a faint field galaxy located some 5 arcsec north-east of PKS 1547−79. The fact that PKS 1547−79 displays higher polarization in the smallest apertures in the present data may indicate that the nuclear regions of this object possess significant intrinsic polarization. A resolution of these uncertainties awaits more extensive multiwavelength polarimetric observations.

Our deep spectrum of this source (Fig. 2a) shows many interesting features. Although this object was thought to be a narrow-line radio galaxy (NLRG) prior to the new observations (Tadhunter et al. 1993), the new spectrum reveals broad components to the permitted Hβ and Mg II λ2800 lines. In addition, the high signal-to-noise ratio continuum spectrum shows no sign of stellar absorption features. While the continuum colours are relatively blue, there is a steep decline in the continuum below 3500 Å. This may result from differential refraction owing to the large zenith distance of these observations.

We have measured the mean continuum fluxes in line-free continuum windows close to the effective wavelengths of the standard U and B broad-band filters in the rest frame of the source. From the flux ratio we derive a $(U-B)$ colour index of −0.50 (±0.02) mag, considerably bluer than the indices of typical elliptical galaxies [for which $0.4 \lesssim (U-B) \lesssim 0.44$ – Shaw & Tadhunter 1994, and references therein]. The reliability of these measures is, however, uncertain given the possibility of differential refraction effects.

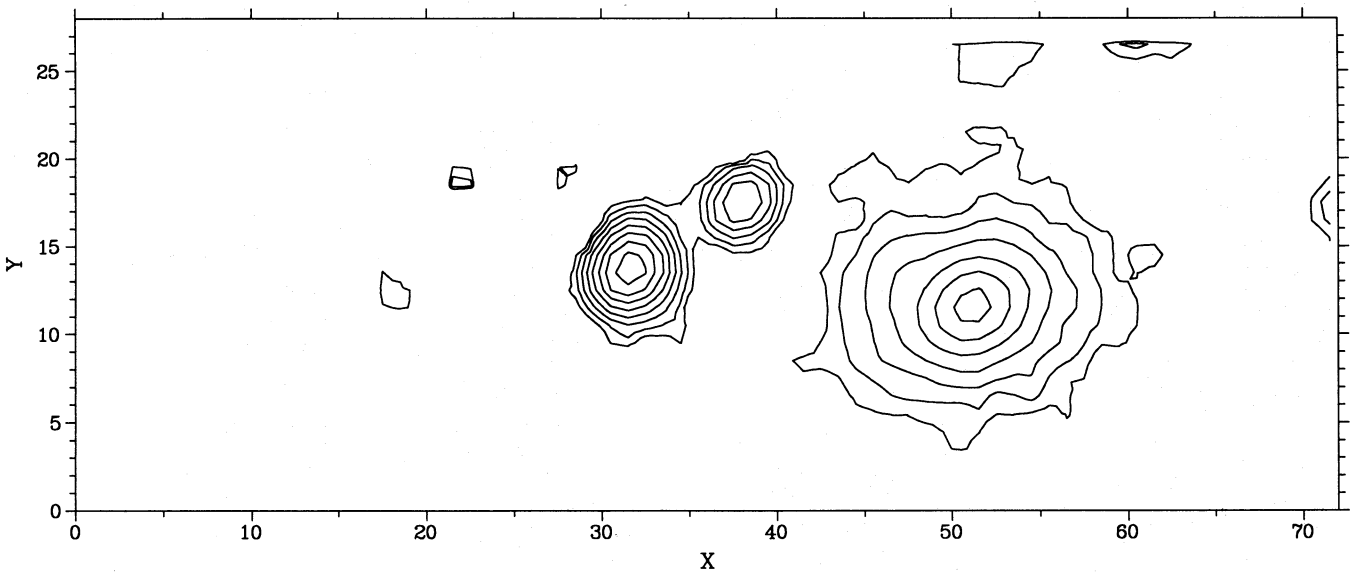

Figure 1. Contour plot of a subregion of the *B*-band polarization image of PKS 1547 − 79 (the object with pixel coordinates $x = 32$, $y = 14$). The contour levels are from 23.5 to 28.3 mag arcsec^{-2} in 0.6 mag arcsec^{-2} intervals. North is up, east to the right and the axes are labelled in pixels (1 pixel = 0.61 arcsec).

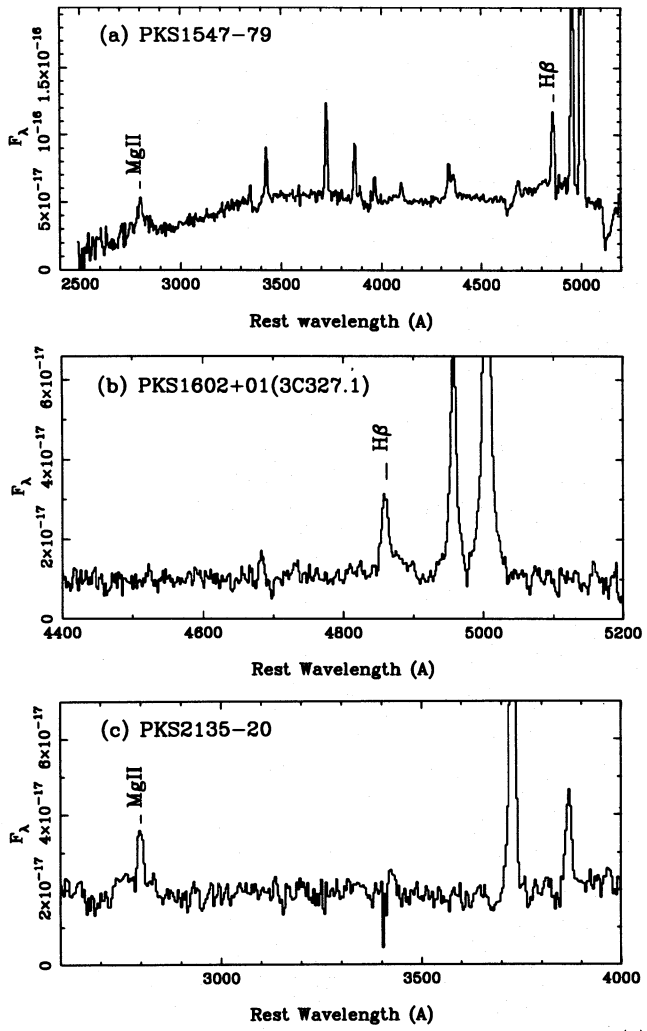

Figure 2. Intermediate dispersion EFOSC and ISIS spectra of (a) PKS 1547 − 79, (b) PKS 1602 + 01, and (c) PKS 2135 − 20, derived as outlined in the text.

3.2.2 *PKS 1602 + 01 (3C 327.1)*

The 4.9-GHz radio structure of this object has a compact, but double-lobed, structure (Morganti et al. 1993), with a position angle of 114° (± 5°). In our direct (*I*-band) EFOSC images, PKS 1602 + 01 possesses a slightly extended nucleus (along the north-east), surrounded by a more diffuse envelope which has an extension towards the south-west. Thus the optical structures of both nucleus and low-surface-brightness envelope are broadly orthogonal to the orientation of the 4.9-GHz radio lobes. The bright, inner regions of PKS 1602 + 01 appear, however, unresolved in the *B*-band polarization frames: the derived FWHM of 1.1 arcsec is equivalent to the estimated seeing at the time of data acquistion.

Two of the observational data sets acquired for this object (i.e. those from night 2) did not use the aperture mask, and the PA = 180° 'o'-ray measures concerned are contaminated by the superposition of a faint field star or galaxy. Correction for this contamination was undertaken in two ways. First, the ratios of (object − sky) fluxes of PKS 1602 + 01 in 'o'- and 'e'-rays were measured for each night in each instrument PA not affected by the contamination. Weighted mean ratios, and associated errors, were thus calculated and these ratios used to derive percentage polarizations and position angles in the usual manner. Such values are given in Table 2.

Evaluation of the reliability of this procedure was undertaken for the second data set acquired on night 2. In this case, integrated (object + sky) fluxes within the contaminating source were measured in each aperture and for all instrument PAs other than 180°. To judge from these measures, the field star or galaxy appears unpolarized. These measures were thus used to predict the likely degree of contamination in the 180° 'o'-ray image of PKS 1602 + 01, and new Stokes parameters were thus evaluated. The polarization measures thus derived agree with those in Table 2 within the uncertainties (for a 6.1-arcsec-diameter aperture $P = 1.3 \pm 2.6$ per cent, while $P = 3.6 \pm 2.3$ per cent in a 4.9-arcsec aperture).

The sensitivity of the derived results to the aperture centring on the contaminating star or galaxy was also evaluated by arbitrary 0.6-arcsec shifts in the adopted location of this source. The polarization measures derived agree with those cited above to within 0.1 per cent ($D = 4.9$ arcsec) and 0.6 per cent ($D = 6.1$ arcsec). Unfortunately, a similar procedure could not be undertaken for the first data set acquired on night 2 owing to the additional superposition of a cosmic ray on the same PA image. Measurements derived from the night 4 data in which the aperture mask was used (and where no superposition occurred) yield equivalent results, however. For apertures of 6.1, 4.9, 3.7 and 2.4 arcsec, $P_{obs} = 1.3\ (\pm 2.5)$, $1.8\ (\pm 2.2)$, $1.9\ (\pm 1.9)$ and $1.8\ (\pm 1.7)$ per cent, respectively.

As Table 2 clearly shows, PKS 1602+01 possesses low measured polarization – we derive a 3σ upper limit of 4–5 per cent polarization in all apertures measured.

Our deep ISIS spectrum of the core of the galaxy (Fig. 2b) shows a broad, blue wing to the Hβ line, which suggests that the object should be classified as a broad-line radio galaxy (BLRG). Another indicator of a genuine BLRG is the relatively large ratio of core-to-total radio flux at 6 cm of 0.061 (Morganti et al. 1993). This is much larger than the typical values for NLRGs (Hine & Longair 1979) but similar to the measured values for the BLRGs.

The $(U-B)$ colour derived from the continuum fluxes in our spectra is $-0.27\ (\pm 0.06)$ mag, again indicating a considerable UV excess when compared to the colours of typical elliptical galaxies.

3.2.3 *PKS 2135−20*

This high-redshift radio galaxy is a CSS. Our direct *B*- and *I*-band EFOSC images show a compact structure which appears unresolved in these data (the FWHM of 1.4 arcsec being identical to the estimated seeing at the time of data acquisition).

To judge from the results in Table 2, this source has low measured polarization at rest-frame UV ($\lambda_{cen} \sim 2680$ Å) wavelengths, our results placing a 3σ upper limit of 2.1–2.7 per cent on the degree of polarization in the UV continuum in this object.

This is another object which was classified as an NLRG based on the earlier spectra (Tadhunter et al. 1993), but which our deep EFOSC spectra show to have broad permitted lines (Fig. 2c). In this case we only detect the broad feature in Mg II λ2800, a WHT/ISIS spectrum of the source at longer wavelengths failing to reveal broad components to Hβ, although the signal-to-noise ratio of the spectrum is not high. The $(U-B)$ colour index derived from the continuum fluxes in these spectra is $-0.29\ (\pm 0.04)$ mag, some ~ 0.7 mag bluer than the colours of typical elliptical galaxies.

3.2.4 *PKS 2250−41*

The broad/narrow-band optical structure and spectroscopy of this striking object are discussed by Tadhunter et al. (1994). It possesses a highly luminous, extended emission-line region west of the nucleus. Although Duncan & Sproats (1992) interpret their 6 cm radio map as that of a gravitational lens candidate, independent 8-GHz observations (Clark et al., in preparation) clearly shows this galaxy to display a classical double-lobed radio morphology with a PA of 97° (±2°).

The nuclear region of this galaxy is significantly polarized. Since the degree of polarization does not change significantly with aperture size despite a factor ~ 2.5 increase in the flux between the largest and smallest apertures (Table 2), it is likely that the polarized light is emitted by an extended region around the nucleus (i.e. not just by an unresolved nuclear component).

A correction for emission-line contamination of 20 per cent yields a mean polarization, averaged over all apertures, of 4.8 (±0.4) per cent. We derive a mean position angle (from a weighted mean of the Stokes parameters for all aperture measures in this table) of 155°.1 (±2°.6). Thus the misalignment between radio and optical polarization position angles is 58°.1 (±3°.3). Applying ellipse-fitting techniques to our direct *B*-band EFOSC images of PKS 2250−41, we find the nucleus to be elongated: over 2.1–5.2 arcsec diameter apertures the mean ellipticity is 0.74 (±0.06) along a position angle of 79°.3 (±4°.5). Optical continuum and polarization position angles therefore differ by 75°.8 (±5°.2). [Note that the polarization position angles do not correspond to those quoted in Tadhunter et al. (1994) as the present measures have been recalibrated, and are also derived from weighted means for all apertures, rather than simply the 3.7-arcsec-diameter aperture used previously.]

As the *B*-band images are dominated by the UV continuum in this object (Tadhunter et al. 1994), these results concur with previous findings for other radio galaxies, that the UV continuum polarization position angle is more orthogonal to that of the optical structure axis than to the radio axis (Cimatti et al. 1993).

The extended emission-line lobe ~ 6 arcsec west of the nucleus has low measured polarization: we derive a 3σ upper limit of 3.9 per cent following correction of 40 per cent for emission-line contamination. As the Stokes parameters derived from the position angle 135° and 180° images of the unmasked night 2 data appear spuriously large, we have also calculated the weighted mean polarization measures after combining night 1 (unmasked) and night 4 (masked) alone. P_{obs} varies from 0.4 (±0.9) per cent (within a 4.9-arcsec aperture) to 0.8 (±0.8) per cent (within a 3.7-arcsec aperture).

An independent estimate of likely Galactic contribution to the polarization was derived using polarization measurements of a faint field galaxy located ~ 11 arcsec north-east of the nucleus. This galaxy has low polarization: within 3.7 and 2.4 arcsec diameter apertures we find 1.9 (±1.7) and 0.5 (±2.1) per cent respectively.

In contrast to the other objects discussed in this paper, our deep spectra show no evidence for broad wings to the permitted lines in either the nuclear or extended regions of this object (see Tadhunter et al. 1994). However, the $(U-B)$ colour indices derived from continuum flux ratios in our spectra are $+0.09\ (\pm 0.05)$ mag and $-0.86\ (\pm 0.05)$ mag for the nucleus and west lobe respectively. Both components therefore show considerable UV excesses when compared with typical elliptical galaxies.

4 DISCUSSION

Many previous studies of the optical polarization properties of radio galaxies have used the *V* band, which is likely to

suffer considerable dilution by the unpolarized light of the old stellar populations in the host galaxies. We have specifically attempted to circumvent this problem by using the *B* band (rest-frame UV) for our work. Our spectra also allow us to make accurate estimates of the emission-line contamination of the *B*-band polarization measurements, and we generally find that such contamination is small ($\lesssim 20$ per cent).

In spite of the fact that measurements were made in the rest-frame UV, and are not significantly affected by emission-line contamination, we find that two of the four radio galaxies presented in this paper display low polarizations in their UV continua. Clearly, there exists a class of powerful radio galaxies which display low rest-frame UV polarizations, other examples of this class being 3C 411 and 3C 441 (Tadhunter et al. 1992).

It is significant that our new spectra show both PKS 1602+01 and 2135−20 to be BLRGs. Our deep ISIS+WHT spectrum of 3C 411, presented in Fig. 3, shows that this object is also a BLRG with broad wings to the Hβ (see also Spinrad et al. 1975). Unfortunately, the existing spectra for 3C 441 are of too poor quality to allow a search to be made for broad permitted lines in that case. Furthermore, the polarimetry observations of 3C 441 were made at longer wavelengths than was the case for the other objects, so that there is a possibility of substantial dilution by the old stellar populations (see Tadhunter et al. 1992). It is unclear, therefore, whether 3C 441 should be classed with the other objects.

Leaving 3C 441 aside, we conclude that a large fraction of the objects with low UV polarization are BLRGs. In these cases it is likely that we are observing the nucleus directly, rather than by scattered light. Previous studies of the optical polarization properties of low-redshift BLRGs (Antonucci 1984) and radio-loud quasars (Stockman, Angel & Miley 1979), show that many of these objects have measured optical polarizations at the level of a few per cent or less, despite negligible dilution by starlight. In such cases the polarization *E*-vectors tend to align parallel to the radio axes (Stockman et al. 1979; Antonucci 1984), and we would predict a similar parallel alignment in PKS 1602+01, PKS 2135−20 and 3C 411, although the existing measurements are not sufficiently accurate to test this prediction.

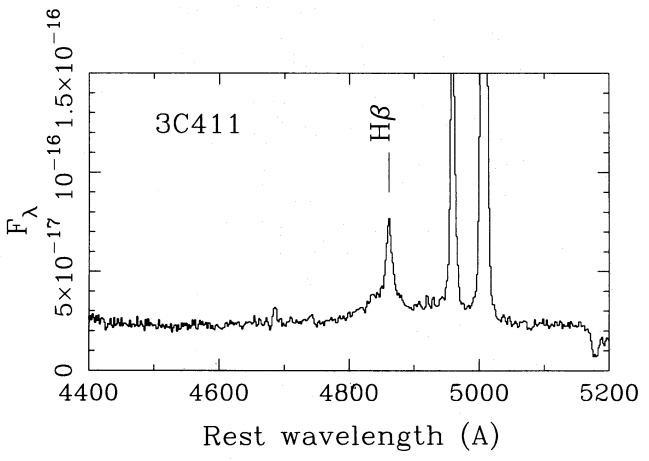

Figure 3. Intermediate dispersion ISIS+WHT spectrum of 3C 411.

It is important to note that, although low UV polarization may be a strong sign that the object is a BLRG in which we are observing the AGN directly, the converse is not true: the detection of broad permitted lines does not necessarily imply that the polarization is low. Indeed, a minority of BLRGs are highly polarized. In these polarized BLRGs it is likely that we are observing the BLR either by scattering (e.g. 3C 234: Antonucci 1984) or by transmission through a dusty medium (e.g. 3C 109: Goodrich & Cohen 1992). The relationship between the broad-line character of the nucleus and the measured polarization is therefore rather subtle and depends on the way the nucleus is observed.

In the present sample, only the (single) narrow-line object in our sample displays unambiguous measurable intrinsic polarization. In common with the majority of other NLRGs, the polarization position angle is approximately orthogonal to the major axis of the UV continuum structure. This result is consistent with the scheme in which the UV excess results from scattering of radiation from a hidden nucleus (Tadhunter et al. 1988; Fabian 1989).

To summarize, a primary result of the present study is the identification of a diversity of UV polarization properties in powerful radio galaxies at intermediate redshifts. In consequence, the UV excesses observed in these objects are unlikely to result solely from scattered light.

5 CONCLUSIONS

In this paper we present polarimetry measurements in the rest-frame UV for four intermediate-redshift ratio galaxies. Deep optical spectra show that three of these objects are broad-line radio galaxies.

In the majority of objects, we measure low polarizations. The low measured polarizations for two of the broad-line objects (PKS 1602+01 and PKS 2135−20) are consistent with the hypothesis that we are viewing their respective broad-line regions directly. The level and orientation of the polarization in the single narrow-line object in our sample (PKS 2250−41) is consistent with scattered AGN light.

One object in our sample (PKS 1547−79) is highly polarized, significantly reddened and also possesses broad-lines. However, there appears to be considerable foreground (Galactic) polarization, and we cannot claim to identify significant intrinsic polarization within this object.

We thus identify a diversity of polarization properties for intermediate- and high-redshift radio galaxies. Clearly, the anisotropic scattering model cannot explain the observed UV excesses in all radio galaxies – particularly the broad-line objects. Direct AGN light, transmitted AGN light and/or intrinsic mechanisms associated with the extended emission line regions (see Dickson et al. 1994) may all contribute at some level.

Unfortunately, all samples of intermediate- and high-redshift radio galaxies observed polarimetrically to date are heterogeneous, being biased towards the brightest, most spectacular objects. The effects of dilution by light from an old stellar population are also significant in the majority of *V*-band observations for objects with $z \lesssim 0.5$. Future progress in understanding the relative importance of the underlying continuum emission mechanisms for the UV continua therefore requires a polarization survey of a complete, unbiased sample of radio galaxies.

ACKNOWLEDGMENTS

MAS and RD were supported by PPARC during the course of this work. We thank Mike Scarrott for useful discussions.

REFERENCES

Antonucci R., 1984, ApJ, 278, 499
Barthel P., 1989, ApJ, 336, 606
Begelman M. C., Cioffe D., 1989, ApJ, 345, L21
Burstein D., Heiles C., 1982, AJ, 87, 1165
Chambers K. C., Miley G. K., van Breugel W., 1987, Nat, 329, 604
Cimatti A., di Serego Alighieri S., Fosbury R., Salvati M., Taylor D., 1993, MNRAS, 264, 421
Daley R. A., 1992, ApJ, 386, L9
de Young D. S., 1989, ApJ, 342, L59
Dickson R., Tadhunter C., Shaw M., Clark N., Morganti R., 1995, MNRAS, 273, L29
di Serego Alighieri S., 1989, in Grosbøl P., Murtagh F., Warmels R., eds, Proc. 1st ESO/ST-ECF Data Analysis Workshop, ESO Conf. & Workshop Proc. 31, p. 1
Duncan R., Sproats L., 1992, Proc. Astron. Soc. Aust., 10, 16
Fabian A. C., 1989, MNRAS, 238, 41P
Goodrich R., Cohen M., 1992, ApJ, 391, 623
Hine R., Longair M., 1979, MNRAS, 188, 111
Lilly S., Longair M., 1984, MNRAS, 211, 833
McCarthy P. J., van Breugel W., Spinrad H., Djorgovski S., 1987, ApJ, 321, L29
Morganti R., Killeen N., Tadhunter C., 1993, MNRAS, 263, 1023
Rees M. J., 1989, MNRAS, 239, 1P
Serkowski K., Matthewson D., Ford V., 1975, ApJ, 196, 261
Shaw M., Tadhunter C., 1994, MNRAS, 267, 589
Simmons J., Stewart B., 1985, A&A, 142, 100
Spinrad H., Smith H., Hunstead R., Ryle M., 1975, ApJ, 198, 7
Stockman H., Angel J., Miley G., 1979, ApJ, 227, L55
Tadhunter C. N., Fosbury R. A. E., di Serego Alighieri S., 1988, in Maraschi L., Maccacaro T., Ulrich M.-H., eds, BL Lac Objects: Proc. Como Conf. 1988. Springer-Verlag, p. 79
Tadhunter C., Scarrott S., Draper P., Rolph C., 1992, MNRAS, 256, 53P
Tadhunter C., Morganti R., di Serego Alighieri S., Fosbury R., Danziger I., 1993, MNRAS, 263, 999
Tadhunter C., Shaw M., Clark N., Morganti R., 1994, A&A, 288, L21
Tinbergen J., Rutten R., 1992, ING User Manual, XXI
Turnshek D., Bohlin R., Williamson R., Lupie O., Koornneef J., Morgan D., 1990, AJ, 99, 1243
Wall J., Peacock J., 1985, MNRAS, 216, 173